PAPER • **OPEN ACCESS**

Contact resistance, coupling and hysteresis loss measurements of ITER poloidal field joint in parallel applied magnetic field

To cite this article: J Huang *et al* 2022 *Supercond. Sci. Technol.* **35** 025016

OPEN ACCESS
IOP Publishing
Superconductor Science and Technology
Supercond. Sci. Technol. **35** (2022) 025016 (13pp)
https://doi.org/10.1088/1361-6668/ac4201

Contact resistance, coupling and hysteresis loss measurements of ITER poloidal field joint in parallel applied magnetic field

J Huang[1,*], Y Ilyin[2], W A J Wessel[1], R Lubkemann[1], H J G Krooshoop[1] and A Nijhuis[1]

[1] Faculty of Science & Technology, University of Twente, Enschede 7522 NB, The Netherlands
[2] ITER International Organization, Saint-Paul-lez-Durance 13067, France

E-mail: j.huang-2@utwente.nl

Received 26 August 2021, revised 25 November 2021
Accepted for publication 10 December 2021
Published 7 January 2022

Abstract

The inter-strand contact resistance and AC losses were measured on an International Thermonuclear Experimental Reactor (ITER) poloidal field (PF) coil joint in a parallel applied AC magnetic field. In addition, the hysteresis loss was measured as a function of the angle with the applied magnetic field on a niobium-titanium (NbTi) strand of the same type as in the joint with a vibrating sample magnetometer. The AC loss measurements were performed at four applied field conditions for combinations of 0 or 1 T offset field and 0.2 or 0.4 T sinusoidal amplitude. The hysteresis loss of the joint was compared with the measured AC loss density of the NbTi strand for the same field conditions as the joint AC loss measurement but with varying the angle of the applied field. The subsequent cable twist angles affect the hysteresis loss since the critical current and penetration field depend on the angle of the applied field. It is found that 15.5° is an effective angle for the calculation of the hysteresis loss of joint when compared to the single strand measurement. The inter-strand contact resistance measurements cover all the typical strand combinations from the five cabling stages of the individual conductors, as well as the strand combinations across the two conductors to characterize the inter-strand including the copper sole resistivity. It is the first time to measure the contact resistances and AC losses of the full-size ITER PF joint. By comparing the measured and simulated data in the JackPot-ACDC model, it is also the first time to obtain the accurate inter-strand, inter-petal and strand to copper sole contact resistivities, which are the main input parameters for the further quantitative numerical analysis of the PF joints, in any current and magnetic field conditions.

Keywords: ITER, poloidal field, joint, contact resistance, AC loss, hysteresis loss

(Some figures may appear in colour only in the online journal)

* Author to whom any correspondence should be addressed.

1. Introduction

The International Thermonuclear Experimental Reactor (ITER) magnet system consists of six poloidal field (PF) coils, all coils are wound with niobium-titanium (NbTi) cable-in-conduit conductors (CICCs) cooled by forced flow liquid helium. The winding connections within and between the double pancakes, as well as to the conductor terminals of the feeder system, are achieved by using twin box lap type joints [1, 2]. The joints undertake a superconducting to non-superconducting state transition due to the copper sole in between the two conductors, both AC and resistive losses are produced by the induced and transport currents, which leads to an increase of the helium temperature. Because of the relatively low critical temperature of the NbTi strand, giving a limited operating margin, the current non-uniformity is a concern for a premature quench of the coils. The current non-uniformity is driven by variation in the resistive and inductive coupling of strand-to-strand and strand-to-copper sole contacts in joint and conductor. The current distribution in the PF coil conductors and joints is mostly inductance-dominated due to the pulsed operating mode [3]. In the case of large current unbalance, the overloaded strands may exceed the critical current and generate a current sharing voltage. Then the distribution of the contact resistances between strands or strand to copper sole determines the current redistribution, and drives the current from the uppermost to less loaded strands [4].

The electromagnetic and thermal properties of the CICCs and the joints can be assessed by a numerical code called JackPot-ACDC developed at the University of Twente [5]. In the code, the cable and joint configuration and the material properties are fixed input parameters, there are no free input parameters except for the input contact resistivities and heat transfer coefficients. These are usually derived from experiments, however, until now there are no experimental data for the full-size ITER PF joint. One of the main motivations of the measurements described in this paper is to obtain the contact resistivities for processing the numerical analysis of the qualification measurements performed in the SULTAN facility, in order to understand and quantify the phenomena related to overloaded strands, AC loss and stability in a transient field [6].

An ITER PF Coil joint sample (named PFJEU6) manufactured with PF5 type conductor [7] at CNIM (France) was first tested in the SULTAN facility (Switzerland) for DC transport current and transverse applied field AC loss properties [8]. It was then shipped to CEA Cadarache (France) for the pressure drop measurements, then delivered to the University of Twente (The Netherlands), to measure the inter-strand, inter-petal and strand to copper sole contact resistances (R_c) and AC losses in parallel alternating magnetic field. In addition, the hysteresis loss of the joint was further detailed by means of measuring the magnetization loops of the NbTi strand with a vibrating sample magnetometer (VSM).

2. Experimental setups and sample preparation

The part of the PFJEU6 joint sample delivered to the University of Twente and its dimension are shown in figure 1, the total length is about 1700 mm, of which the lengths of the joint-box region with stainless steel and the conductor sections outside are 580 and 1120 mm respectively. The PF5 CICC is a circle-in-square shape with outer stainless steel jacket dimension of 52 × 52 mm, the outer and inner diameter of the superconducting cable are 35.3 and 10.0 mm respectively [7]. In the twin box lap type joint, two pieces of copper sole are bonded together with a shim layer in between [1]. For the PFJEU6 joint, the minimum thickness of the copper parts between the two cables is 20.1 mm, including a shim layer with thickness of 7.1 mm, and the resistivity of the copper sole and shim are the same, $\rho = 3.34$ nΩm at $T = 4.5$ K. After specific preparations, the cable end is inserted into a bimetallic box bonded by explosive technology and compacted to fabricate a termination. Two terminations with a copper shim in between are soldered together to form the electrical connection [9]. The axial- and cross-sections of one termination are shown in figure 2, including a cross-sectional view of the PF5 conductor. The shaded area represents the strands, the different areas along the length show the compacted conductor in the bimetallic box with a void fraction of 19% at left and towards the right, a gradual increase to the nominal CICC void fraction of 34%. The effective length of the compacted cable section is around 500 mm, which is similar to the length of the contact with the copper sole.

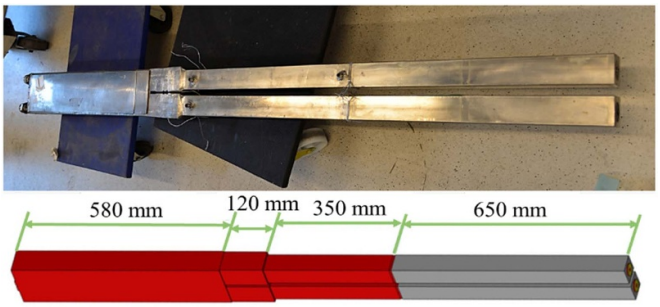

Figure 1. ITER PF5 joint sample (PFJEU6) before measurements (top) and the dimensions (bottom).

2.1. Contact resistance measurement

The contact resistance measurement is performed before the AC loss measurement. The CICC sections with a length of 650 mm, shown in grey colour in figure 1, are cut first. Then, the jackets of the remaining 350 mm long cable sections are removed by a milling machine. The PF5 conductor consists of 1152 NbTi strands evenly distributed in six petals P1–P6. The scheme of the strand selection in one cable is shown in figure 3, with 33 strands selected from each cable, and marked as AR1-33 and BR1-33 for cable A and B respectively. All other superconducting and copper strands of both cable sections outside the joint section are cut shorter, and their cable and sub-cable wraps are removed. Not only the combinations of strands within the cables, like the inter-strand resistance from the first to fourth cabling stages and the inter-petal resistance from the fifth stage, are measured, but also cable to

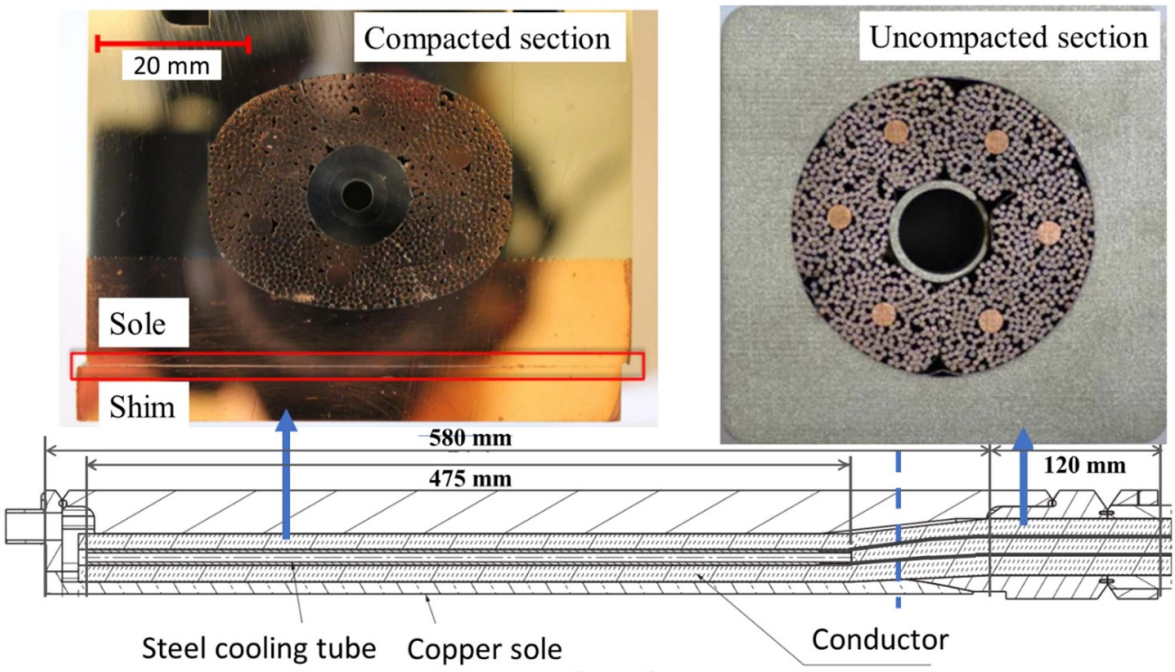

Figure 2. Axial- and cross-sections of one PF termination (half joint), the conductor got compacted in the bimetallic box and transited to the normal configuration outside the box region.

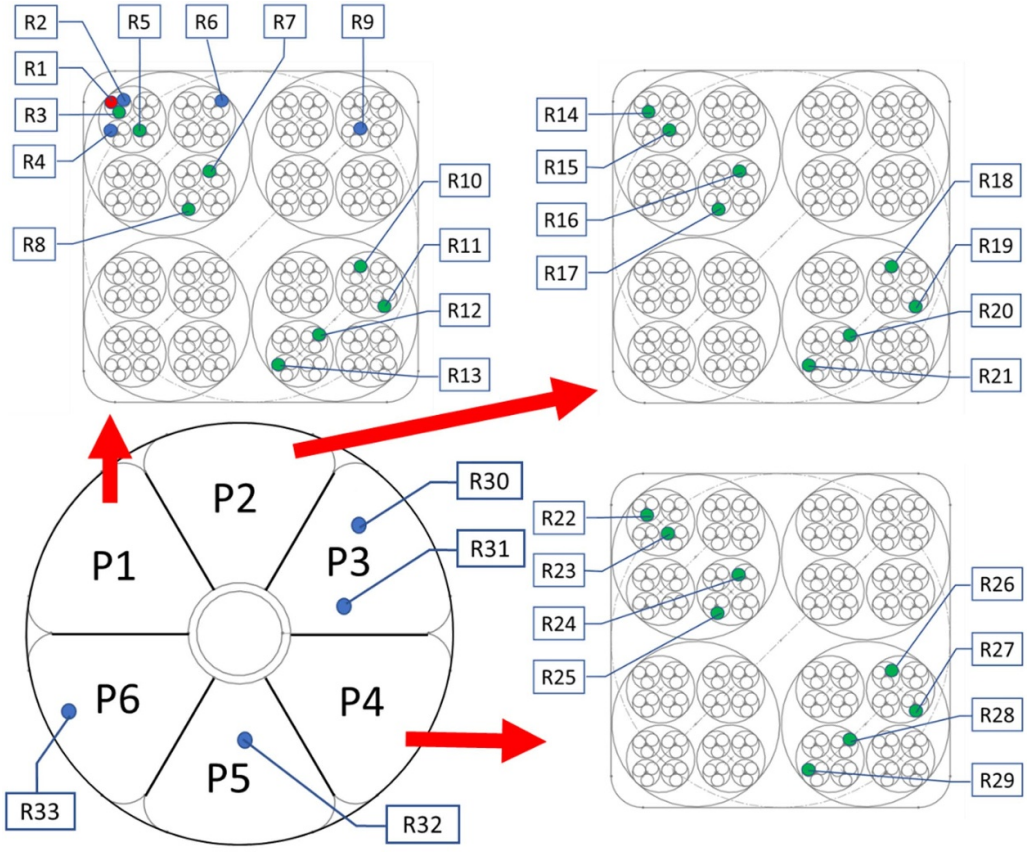

Figure 3. Scheme of strand selection in one cable for contact resistance measurement, the two cables are following the same scheme.

Figure 4. Scheme of current leads (SI1–3) and voltage taps (SV1–3) selection on the copper shim of the joint, view from the side face of joint.

Table 1. Combinations of superconducting strands or current leads on the copper sole of the PFJEU6 joint, for different types of contact resistance measurements.

Inter-strand resistance (strands from cable A or cable B)	
Stage 1	R1–R2, R1–R3, R2–R3.
Stage 2	R1–R4, R1–R5, R7–R8, R10–R11, R12–R13, R14–R15, R16–R17, R18–R19, R20–R21, R22–R23, R24–R25, R26–R27, R28–R29.
Stage 3	R1–R6, R1–R7, R1–R8, R5–R6, R5–R7, R14–R16, R18–R21, R22–R24, R26–R28.
Stage 4	R1–R9, R1–R11, R5–R10, R14–R18, R22–R26.
Stage 5	R3–R14, R3–R16, R3–R18, R3–R21, R3–R22, R3–R24, R3–R26, R3–R28, R3–R31, R3–R32, R10–R14, R10–R16, R10–R18, R10–R21, R10–R22, R10–R24, R10–R26, R10–R28, R14–R24, R14–R26, R14–R28.
Strand to copper sole resistance	
	R1–SI1, R1–SI2, R1–SI3, R16–SI1, R16–SI2, R16–SI3, R26–SI1, R26–SI2, R26–SI3.
Cable to cable resistance (strands from two cables)	
	AR1–BR1, AR1–BR5, AR1–BR22, AR1–BR26, AR3–BR7, AR3–BR9, AR3–BR11, AR3–BR30, AR16–BR16, AR16–BR20.

cable and strand to copper sole resistances are measured. The latter is done by means of selecting a superconducting strand and one of the current leads attached on the copper sole. The scheme of the current leads and voltage taps on the copper sole/shim is shown in figure 4. Three current lead and voltage tap groups are evenly distributed along the joint axis and in the middle of the joint, where the stainless-steel jacket is removed by milling. Small but deep holes are drilled on the exposed copper sole/shim, then the current lead and voltage tap are separately inserted into the holes and pressed tightly to obtain a direct copper to copper electrical contact without using any solder, the assembly is also displayed in figure 6. Finally, the combination of all the three types of contact resistance measurements is summarized in table 1.

The contact resistance is measured by selecting a pair of strands and performing a four-point measurement with an input current of 50 A [10, 11]. For the inter-strand or inter-petal resistance measurements in a specific CICC, the contact resistance is defined as

$$R_c = \frac{V}{I} \cdot l \ [\Omega\mathrm{m}], \tag{1}$$

where V is the measured voltage, I is the applied current through the selected strands and l is the length of the compressed conductor section, for this PF5 joint, $l = 0.50$ m. For the strand to copper or cable to cable resistance measurement, due to the current path across the copper sole, an overall measured resistance with unit of Ω is adopted instead of the normalized resistance with unit of Ωm.

In order to analyze the effect of a magnetic field on the inter-strand resistance and possible influence of the superconductivity of the solder, the joint sample is placed inside a superconducting solenoidal magnet providing a DC background field. The current leads and voltage taps are connected through a switchboard outside the cryostat. The final assembly of the setup and sample is shown in figure 5, including the specific electrical connections of the current leads and voltage taps.

2.2. AC loss measurement

The AC loss measurement is performed after the contact resistance measurement. The conductor sections outside the joint-box region, as shown in figure 1, are cut by spark erosion to its final length of 580 mm.

The measurement is carried out at 4.2 K in liquid helium bath at atmospheric pressure, and in the solenoidal magnet used for the contact resistance measurement, as shown in figure 5. The magnet provides a sinusoidal modulation field with amplitudes of $B_{ac} = 0.2$ or 0.4 T and an offset field of $B_{dc} = 0$ or 1 T, in a direction parallel to the joint axis. The field frequency ranges are 1–160 and 1–85 mHz for the

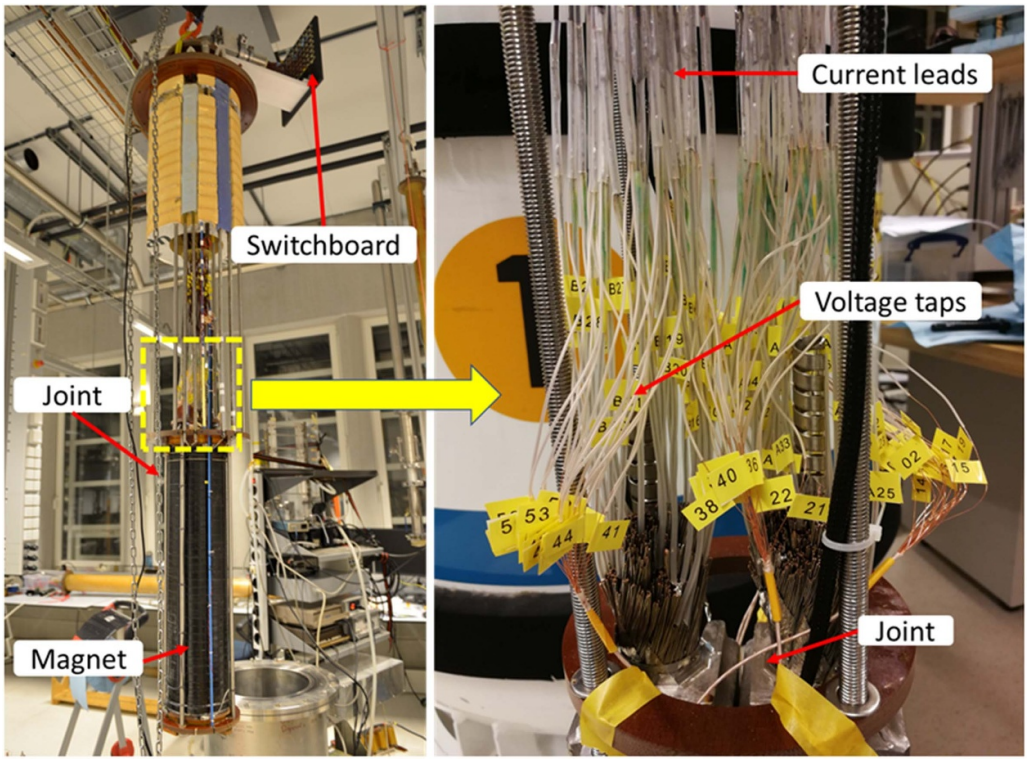

Figure 5. Test setup for the contact resistance measurement of the ITER PFJEU6 joint sample with the electrical connections of current leads and voltage taps.

0.2 and 0.4 T field amplitudes respectively. For the AC loss measurement, the joint sample is placed inside the calorimeter chamber, which is used for measurement of the evaporated helium produced during the power dissipation in the joint. Then the whole object is inserted into the solenoidal magnet as shown in figure 6. The length of the sample is 580 mm but the effective contacting length of the compressed cable with the copper sole is only about 500 mm. The uniform magnet field zone length above 98% is about 480 mm, the schematic of the assembled joint in comparison with the field profile of the AC magnet is shown in figure 7.

The AC loss is measured by two methods simultaneously. One is a calorimetric method measuring the evaporated helium gas flow with a mass flowmeter, then the heat generation is obtained by a calibrated relation to the measured flowmeter voltage. The other is a magnetization method using a pick-up coil that is wound around the joint sample and aligned to the middle plane of the compressed joint-box section. Three compensation coils are located at the top, middle and bottom of the sample respectively. The three different locations of the compensation coils are chosen to evaluate the influence of the position used for the compensation. The relative locations of the four coils with respect to the assembled joint is shown in figure 6. After subtracting the signal of the compensation coil from the pick-up coil the magnetization induced in the sample is calibrated against the calorimetric data.

2.3. Hysteresis loss measurement

The PFJEU6 joint sample AC loss was measured in the SULTAN facility and at the University of Twente, with transverse and parallel applied AC field, respectively. The angles between the superconducting strands and the magnetic field are varying periodically with the twisting pattern of the subsequent cabling stages. The critical current depends on the direction of the applied magnetic field [12, 13], thus it is necessary to analyze the angular dependence of the hysteresis loss in the NbTi strand to make an accurate assessment of the coupling loss.

The University of Twente received from ITER IO, 10 m of PF5 type strand. The hysteresis loss of the joint sample is estimated by measuring the unit magnetization of a short NbTi strand sample and scale it to the total volume of superconducting strand in the joint. The specifications of the NbTi strand are summarized in table 2 [14]. The NbTi strand sample, with measured diameter $d = 0.725 \pm 0.001$ mm and length $L = 5.22 \pm 0.01$ mm, is mounted on a PEEK sample holder and covered with Teflon tape for fixation during measurement with a VSM at the University of Twente. The schematic of the sample holder is shown in figure 8.

Seven slots with different angles to the background field are engraved in the platform of the sample holder to hold the strand sample, as demonstrated in figure 8. The specific angles are $\theta = 0$, 15, 36, 45, 54, 75 and 90° with respect to the field B of the VSM magnet.

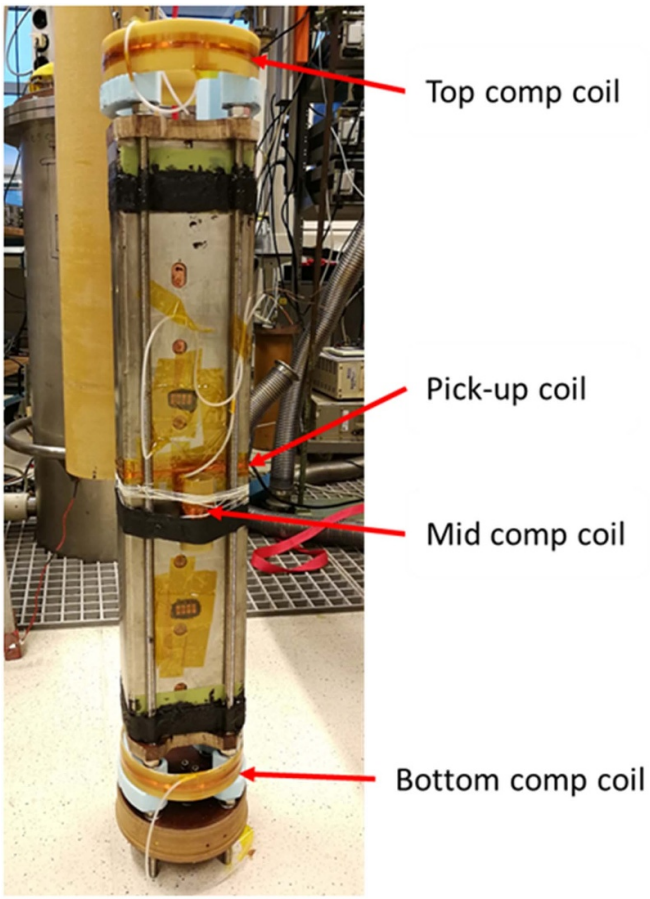

Figure 6. ITER PFJEU6 joint sample for AC loss measurement, one pick-up coil and three compensation coils are instrumented to measure the magnetization of the joint.

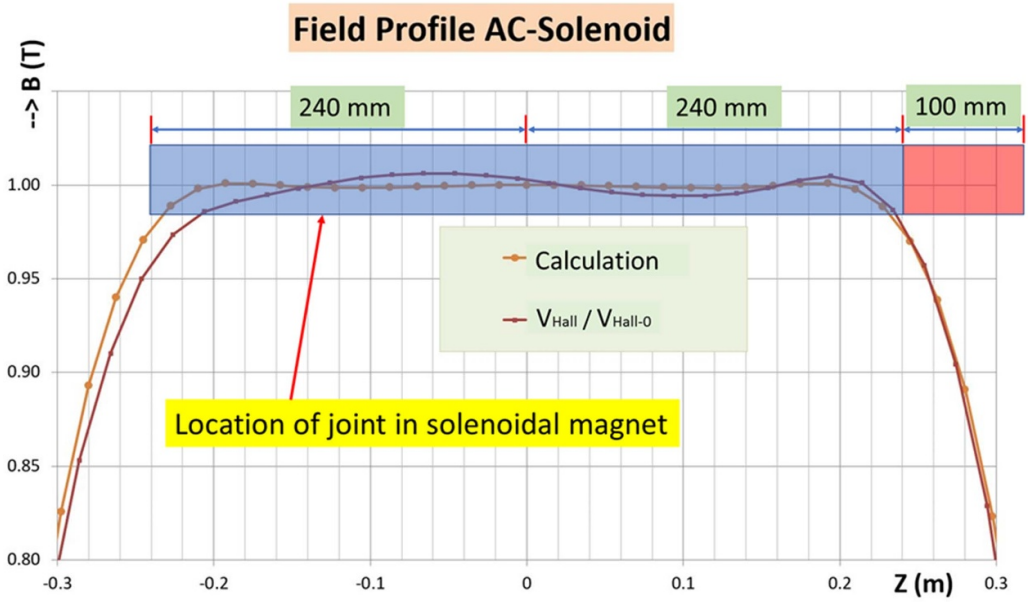

Figure 7. Profile of the AC solenoidal magnetic field and the location of the PFJEU6 joint during the measurement.

Table 2. Main parameters of the tested ITER PF NbTi strand.

Item	Value
Supplier	WST (China)
Strand diameter (mm)	0.730 ± 0.005
Filament diameter (μm)	$\leqslant 8$
Cu:nonCu ratio	2.3
Ni coating thickness (μm)	2
I_c at 5 T, 4.2 K (A)	>339
'n' value at 5 T, 4.2 K	>20
RRR	>100
Hysteresis loss at 4.2 K, $\pm$ 1.5 T cycle (mJ cm^{-3})	<45

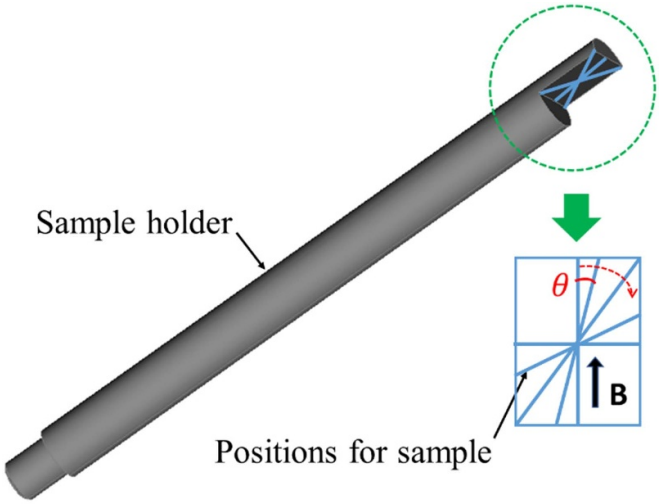

Figure 8. Sample holder for the VSM hysteresis loss measurement. The straight NbTi strand sample is mounted on the platform with different angles θ with respect to the background field B.

The same field conditions as the AC loss measurement of the joint sample, $B_{dc} = 0$ and 1 T and $B_{ac} = 0.2$ and 0.4 T, are taken for the VSM magnetization measurement. The magnetic field applied to the strand sample is continuously swept between the minimum and maximum magnitude with a constant rate of magnetic field change, the operating temperature is also 4.2 K.

3. Experimental results

3.1. Contact resistance measurement in parallel field

The contact resistance is measured with $R_c = V/I$. A series of contact resistance measurements between strands in a triplet is performed in advance, as a function of the input current I up to 50 A, eventually 50 A is selected for the further measurements. Meanwhile, the applied magnetic field increases the average inter-strand resistance due to the magneto-resistance effect of the copper matrix [15], and $B_{dc} = 0.35$ T is applied.

Following the testing scheme from table 1, the inter-strand and inter-petal resistances of strand combinations from the individual cables are measured and the results are shown in figure 9. The average of the resistances from the five individual stages are shown in figure 10. The results show that the inter-strand resistance of cable A is slightly lower than of cable B. The inter-strand resistances from the first to the fourth stage exhibit only a slight increase of 1.5 nΩm. The inter-petal (stage 5) resistance is about 2.5–4.5 larger caused by the stainless-steel foil in between the neighbouring petals [16]. The relatively high and low data correspond to the opposite and neighbouring petal combinations respectively.

In addition to the inter-strand resistance, the current distribution also depends on the strand to copper resistivity. The strand to sole resistivity is assessed by measuring the resistance between a selected strand and a current lead attached to the copper shim layer, as shown in figure 4 and table 1. The resistance between strands from three petals (R1, R16 and R26) and the current leads on the copper sole (SI1, SI2 and SI3) are measured respectively, and the results are shown in figure 11 with resistance unit of nΩ instead of the normalized resistance of nΩm. A spread in resistance is observed, not only for strands within the same cable, but also between the two cables. Depending on the strand path in the cabling pattern and the location of the attached current leads, as shown in figures 4 and 6, the distances between the strand-sole contact point and the respective current lead in the current loops can be quite different, this way causing some spread in resistance.

Another way to assess the strand to copper sole resistance is by measuring two strands, each from both different cables. The strand selection is shown in table 1 and the measured resistances are shown in figure 12. The average strand to strand resistance is about 16 nΩ. The lowest value of 7.5 nΩ is measured on the AR1-BR26 strand pair, this can be compared to the overall joint resistance of 4.8 nΩ, as measured in the SULTAN facility [8].

The inter-strand contact resistance is related to the void fraction of the conductor, the contact resistance decreases as the void fraction decreases [17]. For the PFJEU6 joint, the conductors are compacted from void fraction of 34%–19%. The contact resistance derived from the measurements after 1000 load cycles in SULTAN, as shown in figures 9 and 10, amounts to 2–5 nΩm for the inter-strand resistance and 6–13 nΩm for the inter-petal resistance is. The average resistance of the first and last stage is about 2 and 9 nΩm, respectively.

In order to evaluate the influence of the void fraction on the contact resistances, two prototype full-size ITER PF NbTi conductors (EM1 and EM2) [10], and a full-size Poloidal Field Conductor Insert sample (PFISw) [18, 19] and a sub-size NbTi conductor (sub-size CICC #4) [20] are selected to compare with the PFJEU6 joint conductor. The specification of the four types of conductors and the contact resistances measured with different load conditions are summarized in table 3. Considering the joint sample PFJEU6 has experienced 1000 cycling loads of 165 kN m^{-1} during the experiments in the SULTAN facility, furthermore, the effects of cyclic loading of 165 and 220 kN m^{-1} on the resistance are almost the same, especially after a large number of cycles [10]. A comparison is made with the normal conductors after 1000 cycling loads of 220 kN m^{-1}, the inter-strand (first stage) resistance is 680 and 600 nΩm, and the inter-petal (last stage) resistance is 10 000

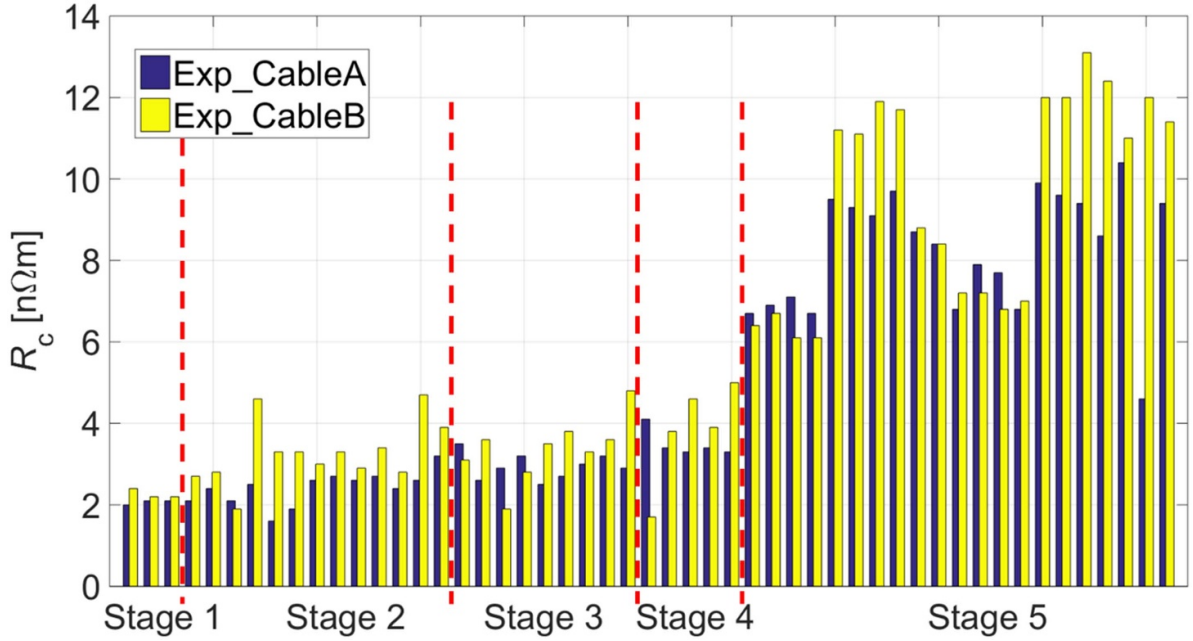

Figure 9. Collection of the inter-strand and inter-petal contact resistances measured between strands from different stages, for the two cables of PFJEU6 joint.

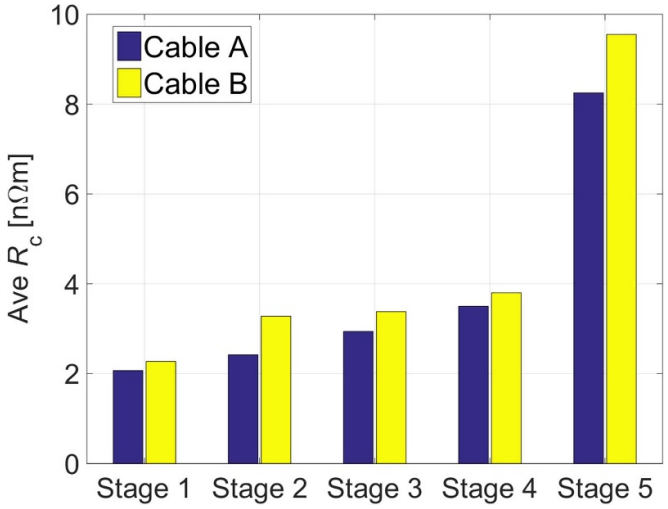

Figure 10. Average inter-strand contact resistance measured between strands from different stages for the two cables of PFJEU6 joint.

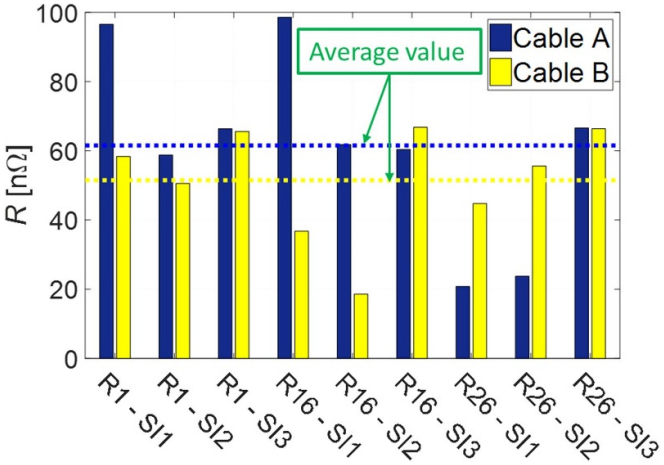

Figure 11. Contact resistance measured between strands in cables and current leads attached to the copper sole.

and 8500 nΩm for EM1 and EM2 respectively. When comparing the resistance behaviour of the joint conductor to the normal conductor after 40 000 cycles from the EM1 and EM2 conductor, the average inter-strand and inter-petal resistance is 65 ((72 + 58)/2) and 2560 ((2960 + 2160)/2) nΩm, being 33 and 284 times larger than the compressed PFJEU6 conductor. Moreover, the ratios of inter-petal to inter-strand resistance are 40 and 4.5 for the regular and compressed conductors, respectively.

For the PFISw conductor with more strands and experienced higher cycling load of 315 kN m^{-1}, the inter-strand and inter-petal resistance after 1000 cycles is 1200 and 2000 nΩm, respectively, while after 40 000 cycles, the inter-strand resistance drops faster than the inter-petal resistance, becomes 45 and 552, respectively, the latter is smaller than EM1 and EM2 probably due to the tighter strand configuration. A sub-size conductor (#4) is compared as well, the magnitude of the first-stage resistance is in accordance with the conductors EM1 and EM2. The last-stage resistance is smaller because it has only four stages, however, the inter-petal to inter-strand ratio is still a relatively high value of 12, like the PFISw conductor.

3.2. AC loss measurement in parallel field

For the pick-up coil magnetization method, there are three compensation coils installed at different positions and one

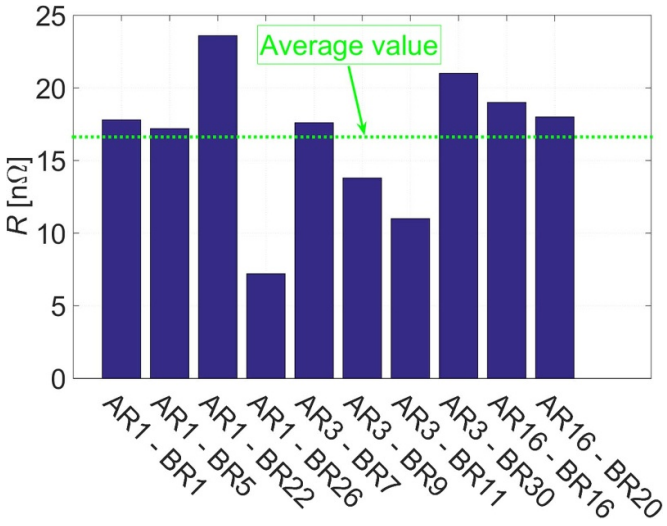

Figure 12. Resistance measured between strands from the two cables.

Table 3. Specification of the NbTi conductors for comparison of the inter-strand contact resistance results with different void fraction measured under different load conditions.

Sample	PFJEU6	EM1		EM2		PFISw		Sub-size CICC #4	
Strand coating	Ni	Ni		Ni		Ni		Ni	
D_strand (mm)	0.73	0.81		0.81		0.73		0.7	
Cu:nonCu	2.3	1.9		1.9		1.41		1.05	
Void fraction	19%	36%		36%		33.5%		35%	
Cable pattern	3/4/4/4/6	3/4/4/4/6		3/4/4/4/6		3/4/4/5/6		(6 + 1)/3/4/4	
Nr. SC strands	1152	1152		1152		1440		288	
Sub-cable wrap	Yes	Yes		Yes		Yes		Yes	
Load (kN m^{-1})	165	220		220		315		200	
Load cycles	1000	1000	40 000	1000	40 000	1000	40 000	1000	40 000
R_c (first stage) [nΩm]	2	680	72	600	58	1,200	45	280	23
R_c (last stage) [nΩm]	9	10 000	2960	8500	2160	2000	552	1240	280

magnetization pick-up coil, as shown in figure 6. A series of tests were carried out first to evaluate the effect of the location of the individual compensation coil on the resulting magnetization signal and then to select the most accurate compensation coil. The bottom compensation coil is quite close to the joint and some magnetic flux induced in the joint is being picked up by this coil. It was decided not to use the bottom coil for further analysis. The AC losses measured by the magnetization method using the middle and top compensation coil and the results obtained from the calorimetric method are shown in figure 13. For the whole frequency range, a good correlation is observed between the data measured by the calorimetric and magnetization method using the signal from the middle compensation coil. Therefore, the middle compensation coil is chosen for processing the AC loss measurements with the magnetization method.

The AC losses of the joint exposed to the four applied magnetic fields, $B_{dc} = 0$, 1 T, $B_{ac} = 0.2$, 0.4 T, are measured by the calorimetric and magnetization method simultaneously and the results are shown in figure 14 with the curves representing the fitting of the magnetization data. The comparison shows a good agreement between the magnetization and calorimetric data. The calorimetric data measured at $B_{apl} = \pm 0.2$ T, a slight discrepancy is observed, most likely caused by a fluctuation in the helium pressure during the measurement.

3.3. Strand VSM hysteresis loss measurement

The magnetic moment m of the NbTi strand sample is directly measured by the VSM, the magnetization M is defined as the moment of a unit volume, $M = m/V$, where V is the volume of the strand sample. Considering the demagnetization effect [21], a calibration with a pure nickel strand is performed, of which the dimension and shape is similar to the NbTi sample [22]. The measured saturation magnetization $\mu_0 M$ of the nickel sample is shown in figure 15 and table 4, with an adjustable angle θ with respect to the applied background field of the VSM, as demonstrated in figure 8. The saturation magnetization of the nickel wires is dependent on the orientation of the applied magnetic field [23, 24], the standard saturation magnetizations of nickel at 4.2 K are derived from previous measurements performed at the University of Twente [25], $\mu_0 M\_ref = 565$ and 646 mT for field in parallel and perpendicular directions respectively. By taking these

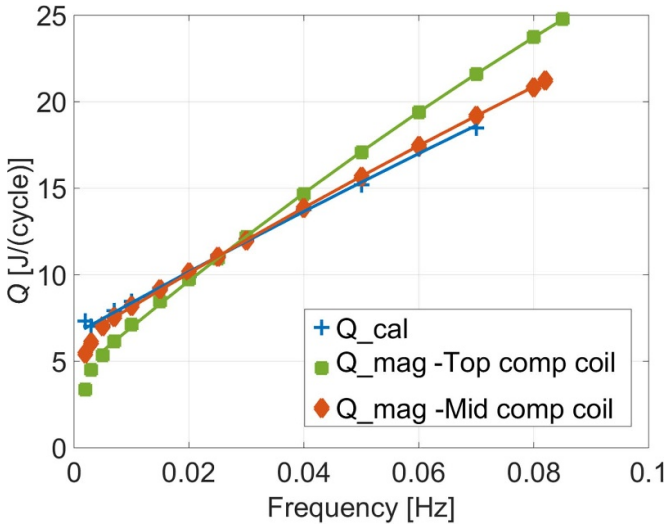

Figure 13. AC losses of the joint measured by the calorimetric method and the magnetization method. The magnetization data are processed with the signals from the Top and Middle compensation coils respectively, the applied field is $B_{dc} = 0$ T, $B_{ac} = 0.4$ T.

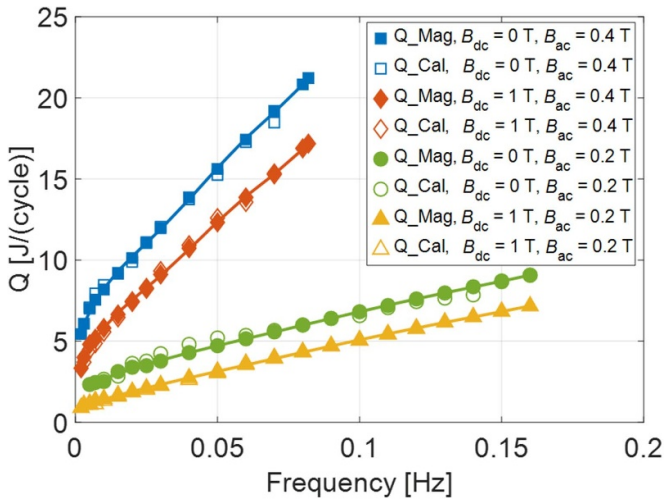

Figure 14. Comparison of the AC losses of the PFJEU6 joint measured by the magnetization and calorimetric methods, using different applied magnetic field conditions.

two referenced saturation magnetizations measured with parallel field at 0° and transverse field at 90°, the corrected saturation magnetizations ($\mu_0 M\_ref$) at the other three angles are derived by interpolation and fitting method, the correction factor defined as $k = \mu_0 M\_ref/\mu_0 M$ is then calculated correspondingly. The saturation magnetizations and correction factors at five angles are listed in table 4.

For the PF5 NbTi conductor, depending on the cabling pattern, the local angle between the strand axis and the applied field is changing periodically with the twist pitches of the different cable stages. The angle distribution (absolute values) along the strand length is calculated with the JackPot-ACDC code [5, 6, 26]. The calculated physical average angle of the compacted joint section is $\alpha = 11.4°$. However, considering the weighted effect of the angle on the hysteresis loss, as

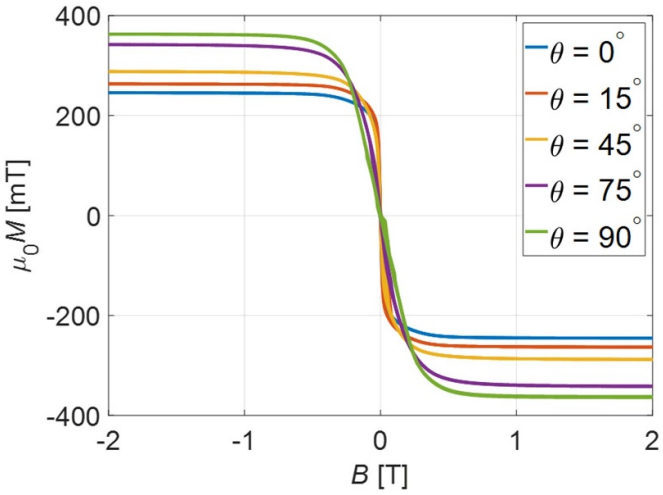

Figure 15. Saturation magnetization $\mu_0 M$ of the nickel sample measured with fields in different directions.

Table 4. Saturation magnetization of the nickel sample measured with VSM, and the saturation magnetization after correction, with applied field orientation in five directions.

Θ	0°	15°	45°	75°	90°
$\mu_0 M$ (mT)	246	264	289	343	363
$\mu_0 M\_ref$ (mT)	565	577	595	632	646
Correction factor k	2.30	2.19	2.06	1.84	1.78

illustrated in table 4, an effective average angle $\beta = 15.5°$, instead of the physical average value $\alpha = 11.4°$, is obtained and applied to calculate the integrated hysteresis loss.

The magnetization of the NbTi strand sample with different magnetic field conditions and different angles is measured, of which the magnetization at $\theta = 15°$ is shown in figure 16, it is used to estimate the hysteresis loss of the joint, with the corresponding saturation magnetization $\mu_0 M\_ref = 577$ mT and correction factor $k = 2.19$.

The hysteresis loss per unit volume of the NbTi sample measured at different field conditions is derived by calculating the area enclosed by the magnetization loop according to equation (2), where the ΔM is denoted as the width of the magnetization loop, $\Delta M(\mathrm{B}) = M^{+}(\mathrm{B}) - M^{-}(\mathrm{B})$ [27]

$$q_{\mathrm{hys}} = \oint M \mathrm{dB} = \int_{-B_m}^{B_m} \Delta M(\mathrm{B})\ \mathrm{dB}\ \left[\mathrm{J/m^3/cycle}\right]. \quad (2)$$

The hysteresis loss of the whole PFJEU6 joint is calculated with equation (3),

$$Q_{hys} = \sum_{i=1}^{N} q_{hys}(i) \cdot V_{NbTi}(i)\ \left[\mathrm{J/cycle}\right], \quad (3)$$

V_{NbTi} is the volume of the NbTi strand intersections, N is the number of all strand intersections in the joint.

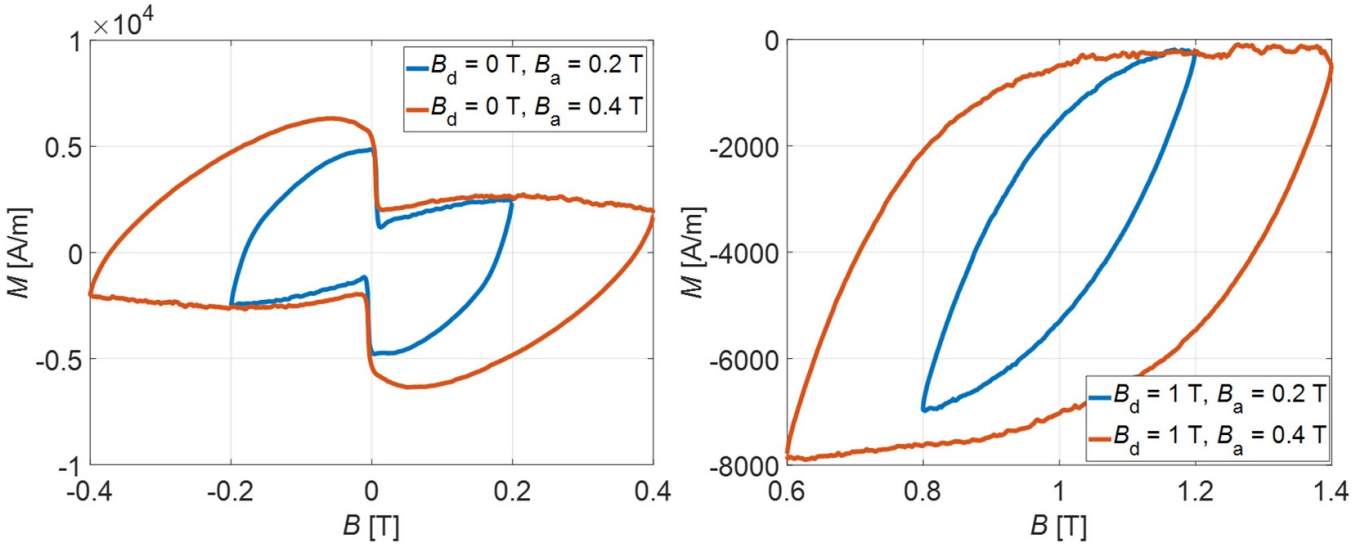

Figure 16. Measured magnetization of the ITER NbTi strand with field angle of 15°, the field amplitude B_{ac} = 0.2 and 0.4 T, and background magnetic field (left) B_{dc} = 0 T, (right) B_{dc} = 1 T respectively.

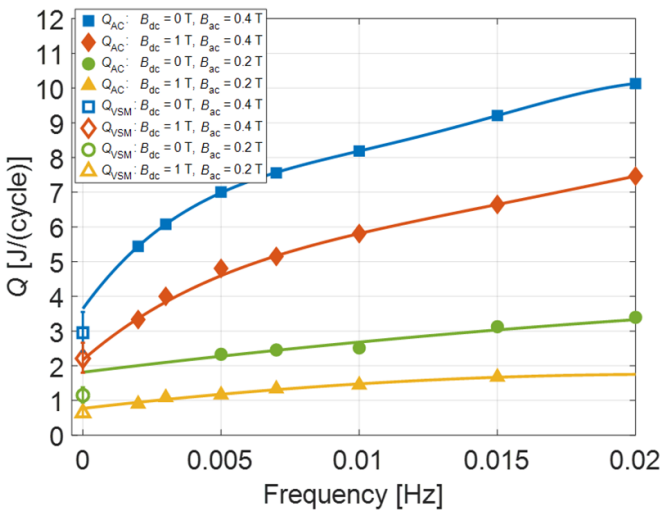

Figure 17. Hysteresis loss estimated from the intercepts of measured AC losses, in comparison with the data from VSM measurements, for different field conditions.

Table 5. Estimation of the hysteresis loss of the joint from the intercepts in AC loss measurements and the VSM measurements, for different field conditions.

B_{dc} (T)	B_{ac} (T)	Q_{vsm} (J cycle^{-1})	Q_{AC} (J cycle^{-1})	Polynomial fit order
0	0.2	1.15	1.81	2
0	0.4	2.95	3.64	4
1	0.2	0.64	0.77	2
1	0.4	2.21	2.17	5

The hysteresis losses (Q_{vsm}) of the sample joint with different magnetic field conditions are calculated and shown in figure 17 and table 5.

The hysteresis losses of the full joint can also be obtained from the intercept of the fitting curves of the measured AC loss data at the low frequencies [26]. For the applied AC magnetic fields, the polynomial fitting curves are derived and shown in figure 17, the corresponding intercepts and fitting orders are listed in table 5. With regard to the hysteresis losses derived from the two methods, a relatively good agreement is observed for applied field conditions with B_{dc} = 1 T, while the values derived from the joint AC loss measurements without DC background are higher than obtained from the VSM measurement. The probable reason for the deviation at low fields is the arbitrary choice of the fitting function, as seen in table 5, the orders of the polynomial fitting curves vary from 2 to 5. Although an underestimation of the VSM measured results at 15° is also possible, which related to the measuring errors like the rotational dependence effect of the sample holder [28], but the error is usually within ±0.5 J cycle^{-1}, thus it is more defined than the arbitrary fitting method employed in the AC loss measurements. Furthermore, the comparison of the hysteresis losses derived from two methods provides a double-check.

4. Conclusion

The contact resistances and the AC loss of the ITER PF5 joint (PFJEU6) are extensively measured in parallel magnetic fields and the angular dependence of the hysteresis loss of the NbTi strand is measured with a VSM.

The inter-strand, inter-petal and strand to copper sole contact resistivities of the two cables of the joint are measured, the resistance spread in cable B is slightly higher than in cable A. The inter-strand resistances (first to fourth stage) are in the range of 2–4 nΩm and increase slightly with subsequent cabling stages. The inter-petal resistance (5th stage) is found to be in the range of 6–12 nΩm, which is about 2.5–4.5 times higher than the inter-strand resistances. The inter-strand and inter-petal contact resistances of the joint are, respectively,

30 and 300 times smaller than for regular (uncompressed) ITER PF conductors. Furthermore, the inter-petal to inter-strand ratio is decreased from 40 to 4.5 as the conductor in the joint is compressed to a void fraction of 19%. The strand to copper sole resistivity is evaluated by measuring the resistance between single strands, each selected from both different cables showing an average resistance of 16 nΩ and a minimal resistance of 7.5 nΩ, while the overall joint resistance was measured as 4.5 nΩ.

The AC loss measurement is performed by magnetization and calorimetric methods with good agreement.

The angular dependence of the hysteresis loss on the applied magnetic field in the CICCs is estimated to support the accuracy of the hysteresis and coupling loss assessment at very low frequencies of the applied field. The hysteresis loss derived at the VSM measurement with an angle 15.5° between the strand axis and field coincides well with the value derived from the intercept of the fitting curve of AC loss measurements.

This is the first time we have measured the contact resistances and AC losses of the full-size ITER PF joint. By comparing the measured and simulated data in the JackPot-ACDC model, it is also the first time to obtain the accurate inter-strand, inter-petal and strand to copper sole contact resistivities, which are the main input parameters for the further quantitative numerical analysis of the PF joints, in any current and magnetic field conditions. The quantitative analysis of the contact resistance on the current redistribution and AC losses is going to be presented in subsequent papers.

Data availability statement

The data generated and/or analysed during the current study are not publicly available for legal/ethical reasons but are available from the corresponding author on reasonable request.

ORCID iDs

J Huang https://orcid.org/0000-0003-1662-4152
A Nijhuis https://orcid.org/0000-0002-1600-9451

References

[1] Lim B, Simon F, Ilyin Y, Gung C Y, Smith J, Hsu Y H, Luongo C, Jong C and Mitchell N 2011 Design of the ITER PF coils *IEEE Trans. Appl. Supercond.* **21** 1918–21
[2] Mitchell N, Devred A, Libeyre P, Lim B and Savary F 2012 The ITER magnets: design and construction status *IEEE Trans. Appl. Supercond.* **22** 4200809
[3] ITER 2006 Design Description Document: Magnet Report
[4] Cau F and Bruzzone P 2009 Inter-strand resistance measurements in the termination of the ITER SULTAN samples *Supercond. Sci. Technol.* **22** 045012
[5] van Lanen E P A and Nijhuis A 2010 JackPot: a novel model to study the influence of current non-uniformity and cabling patterns in cable-in-conduit conductors *Cryogenics* **50** 139–48
[6] van Lanen E P A and Nijhuis A 2011 Simulation of interstrand coupling loss in cable-in-conduit conductors with jackpot-AC *IEEE Trans. Appl. Supercond.* **21** 1926–9
[7] Devred A *et al* 2012 Status of ITER conductor development and production *IEEE Trans. Appl. Supercond.* **22** 4804909
[8] SWISS PLASMA CENTER 2017 PFJEU6 SULTAN sample, test report
[9] Simon F, Boyer C, Ilyin Y, Beemsterboer C and Lim B S 2012 Design of the ITER PF coil joints *IEEE Trans. Appl. Supercond.* **22** 4804104
[10] Nijhuis A, Ilyin Y, Abbas W, ten Haken B and ten Kate H H J 2004 Change of interstrand contact resistance and coupling loss in various prototype ITER NbTi conductors with transverse loading in the Twente cryogenic cable press up to 40000 cycles *Cryogenics* **44** 319–39
[11] van Lanen E P A, Feng L, van Meerdervoort R P P, Wessel W A J and Nijhuis A 2010 Interstrand resistance measurements on the conductor terminations of TFPRO2 and JATF3 SULTAN samples *IEEE Trans. Appl. Supercond.* **20** 474–7
[12] Takayasu M, Montgmery D B and Minervini J V 1998 *Advances in Cryogenic Engineering (Materials)* vol **44** pp 1035–42
[13] Schild T and Cloez H 1998 Magnetic field orientation dependence of critical current in industrial Nb_3Sn strands *Cryogenics* **38** 1251–7
[14] Liu W T, Liu X H, Feng Y, Xie H J, Wang T C and Li J F 2010 Development of fine filament NbTi superconducting strands for ITER *IEEE Trans. Appl. Supercond.* **20** 1504–6
[15] Nijhuis A, Ten Kate H H J, Duchateau J and Decool P 2001 Control of contact resistance by strand surface coating in 36-strand NbTi CICCs *Cryogenics* **41** 1–7
[16] Ilyin Y and Rolando G *et al* 2016 Analysis of ITER PF coil joint design under reference operating scenario *IEEE Trans. Appl. Supercond.* **26** 4201305
[17] Nijhuis A, Ilyin Y, Abbas W, Ten Kate H H J, Ricci M V and della Corte A 2005 Impact of void fraction on mechanical properties and evolution of coupling loss in ITER Nb_3Sn conductor under cyclic loading *IEEE Trans. Appl. Supercond.* **15** 1633–6
[18] Ilyin Y, Nijhuis A, Abbas W, Bruzzone P, Stepanov B, Muzzi L, Gislon P and Zani L 2005 Effect of cyclic loading and conductor layout on contact resistance of full-size ITER PFCI conductors *IEEE Trans. Appl. Supercond.* **15** 1359–62
[19] Bruzzone P *et al* 2005 Test results of the ITER PF insert conductor short sample in SULTAN *IEEE Trans. Appl. Supercond.* **15** 1351–4
[20] Ilyin Y, Nijhuis A, Abbas W and Ten Kate H H J 2011 Electromagnetic performance of sub-size NbTi CICC's subjected to transverse cyclic loading *IEEE Trans. Appl. Supercond.* **14** 1503–6
[21] Panda A K, Basu S and Mitra A 2002 Demagnetisation effect and its correction on the measurement of magnetic hysteresis loop of melt-spun ribbons *J. Magn. Magn. Mater.* **261** 190–5
[22] Quantum Design Company 2010 *Accuracy of the Reported Moment: Sample shape Effects* SQUID VSM application note 1500–015
[23] Raviolo S *et al* 2018 Angular dependence of the magnetic properties of permalloy and nickel nanowires as a function of their diameters *Mater. Res. Express* **5** 015043
[24] Tian F, Zhu J, Wei D and Shen Y T 2005 Magnetic field assisting DC electrodeposition: general methods for high-performance ni nanowire array fabrication *J. Phys. Chem.* B **109** 14852–4
[25] Bergen A 2012 Influence of sample length and orientation on VSM experiments *Report* University of Twente

[26] Nijhuis A and ten Kate H H J 1996 Parametric study on coupling loss in subsize ITER Nb_3Sn cabled specimen *IEEE Trans. Magn.* **32** 2743–6
[27] Seiler E, Richter D, Bordini B, Bottura L, Bessette D, Vostner A and Devred A 2016 Hysteresis losses and effective $J_c(B)$ scaling law for ITER Nb_3Sn strands *IEEE Trans. Appl. Supercond.* **26** 8200307
[28] Quantum Design Company 2010 *Accuracy of the reported moment: axial and radial sample positioning error* SQUID VSM application note 1500-010